PCCP

Pulsed laser deposition of $La_{0.6}Ca_{0.4}CoO_3$ (LCCO) films. A promising metal-oxide catalyst for air based batteries†

M. J. Montenegro,[a] M. Döbeli,[b] T. Lippert,*[a] S. Müller,[a] B. Schnyder,[a] A. Weidenkaff,[c] P. R. Willmott[ad] and A. Wokaun[a]

[a] *Paul Scherrer Institut, CH-5232 Villigen PSI, Switzerland. E-mail: thomas.lippert@psi.ch; Fax: +41-56-3102485; Tel: +41-56-3104076*
[b] *Paul Scherrer Institut c/o ETH Hönggerberg, CH-8093 Zurich*
[c] *University Augsburg, Universitätstr. 1 D-86159, Augsburg, Germany*
[d] *University of Zürich, Winterthurerstr. 190 CH-8057, Zürich, Switzerland*

Received 3rd January 2002, Accepted 16th April 2002
First published as an Advance Article on the web 16th May 2002

$La_{0.6}Ca_{0.4}CoO_3$ (LCCO) thin films were deposited on MgO(001) and stainless steel substrates by pulsed reactive crossed-beam laser ablation (PRCLA). The film stoichiometry was characterized by Rutherford backscattering spectrometry (RBS). The data confirmed that the material transfer from the target to the substrate is congruent. The thickness and surface roughness of the films is in the range of 200–500 and 2–12 nm, respectively, depending on the deposition conditions. The quality of the deposited film was analyzed by X-ray diffraction (XRD) and high resolution transmission electron microscopy (HRTEM). Epitaxial and single oriented thin films could be grown. In view of the importance of the surface composition in electrochemistry, X-ray photoelectron spectroscopy (XPS) measurements were performed. The electrochemical activity of the LCCO films is influenced by the crystallinity of the film.

Introduction

Perovskite type oxides (ABO_3) with high conductivity are promising candidates as catalysts for solid oxide fuel cells[1] and metal-air batteries.[2] The perovskites containing a lanthanide in A and a transition metal in B reveal high catalytic activity for several reactions.[3] Particularly, the perovskites containing Co, Mn, Fe, Cu and Ni show good catalytic activity for oxygen evolution[4] while pyrochlores reveal superior properties for oxygen reduction.[5] The application of LCCO as a bifunctional catalyst, for metal–air batteries was first proposed by Shimizu *et al.*[6] and applied recently in rechargeable zinc/air batteries by Mueller *et al.*[7] To study and compare the mechanism of oxygen reduction/evolution reaction on different perovskites, it is necessary to prepare electrodes on inactive substrates and with well defined electrolyte/oxide interfaces. Dense crystalline films on single crystal substrates would fulfill these requirements. Pulsed laser deposition (PLD) has been successfully applied to the growth of many types of multicomponent thin films of very high quality.[8,9] In our experiments a modified technique, *i.e.* pulsed reactive crossed-beam laser ablation (PRCLA), was applied. In this technique a gas pulse crosses the ablation plume close to its origin (Fig. 1), allowing an increase of gas phase interaction and the probability of reactive scattering, while allowing the resulting species to propagate freely away from the localized scattering region.[8]

Another important aspect of electrocatalysis of perovskite which has not been studied so far, is the influence of the crystallinity on the electrocatalytic activity. Laser based deposition methods have the potential to allow a variation of the crystallinity by changing the deposition conditions. Therefore, various deposition parameters are varied, to test whether and how the film growth can be influenced.

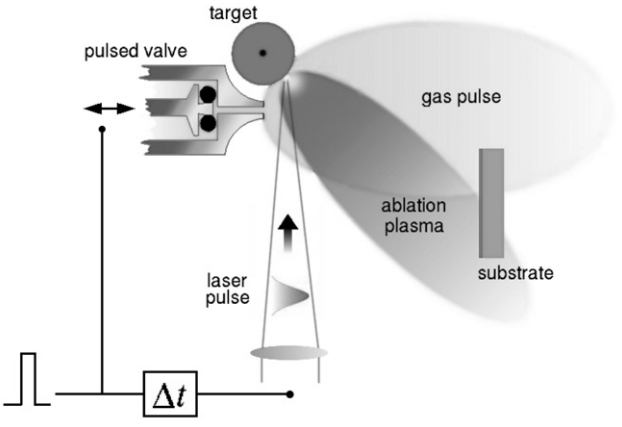

Fig. 1 Scheme of pulsed reactive crossed-beam laser ablation.

Experimental

The PRCLA experimental setup has been described previously in detail.[8,10] LCCO films were deposited using a KrF excimer laser ($\lambda = 248$ nm, 17 ns pulse length, laser fluence 7.6 J cm^{-2} and repetition rate 10 Hz) from a rotating $La_{0.6}Ca_{0.4}CoO_3$ target. The target powder was prepared by spray pyrolysis. The stoichiometry of the target was analyzed and confirmed by atomic emission spectroscopy (AES). The substrate deposition temperature was 650 °C for MgO and 560 °C for stainless steel (SS), with a background pressure of 8×10^{-4} mbar O_2. The gas pulse was generated using a pulsed valve operating at a

† Presented at the LANMAT 2001 Conference on the Interaction of Laser Radiation with Matter at Nanoscopic Scales: From Single Molecule Spectroscopy to Materials Processing, Venice, 3–6 October, 2001.

backing pressure of 2 bar N_2O (99.999% purity, pulse length of 400 μs) and synchronized with the laser pulse using a variable trigger delay. The films were grown on MgO(001), stainless steel (SS) and gold ($10 \times 10 \times 0.5$ mm) substrates. The substrates were rotated during the deposition to obtain uniform film thickness. The surface roughness and film thickness were determined with a Profilometer (Dektak 8000). RBS measurements were performed using a 2 MeV ^{4}He beam[11] and a surface barrier silicon detector. The data were analysed using the RUMP program.[12] Structure, crystalline quality and texture of the films have been studied with a Siemens D5000 X-ray diffractometer with Bragg–Brentano geometry using Cu Kα radiation. The apparatus is equipped with an Eulerian cradle for the sample orientation. The tubular aperture is limiting the beam divergence to 0.3°. Scans in $\theta/2\theta$ geometry under different tilt angles were performed using an aperture of 0.2 mm. X-ray pole figures were measured by rotating the sample around the φ axis and tilting the sample along the χ axis during the measurements with a fixed detector position (2θ). The TEM studies were performed on a Phillips CM 30 apparatus equipped with EDX detector. The cross-sectional samples were prepared by cutting two small squares of the sample and gluing those face to face together. Then they were thinned by mechanical grinding and ion-milling. The XPS data were measured with a Thermo VG ESCALAB 220i XL using monochromatic Al Kα radiation. The gas diffusion preparation has been described previously in detail.[13] The electrochemical activity of the LCCO film and gas diffusion electrodes for the oxygen reactions was measured with a three electrodes arrangement with the LCCO as a working electrode, a Pt-wire as counter-electrode, and an Hg/HgO as reference electrode with a potentiostat (Amel instruments, model 2049). The electrodes are submerged in a cell with KOH 1 M. Oxygen is bubbled through the KOH solution to saturate it. A potential is applied to the electrode, obtaining the current as answer, that is normalized for the electrode area (*i.e.* current density).

Results and discussion

A. Film growth

The increase of the emission intensity of the ablation plume due to its interaction with the N_2O gas pulse is shown in Fig. 2. The plume becomes much brighter and extends further from the point of ablation. The film quality is independent of the number of laser pulses delivered to the target, but with laser fluence above 12 J cm^{-2}, liquid particulates in the micron range (droplets) are ejected from the target and incorporated into the film. The droplet formation at higher laser fluences is explained by splashing from a molten layer on the target.[14] Below this energy density, no droplets were detected. The most important factor for the growth of LCCO films without oxygen deficiency is the combination of oxygen background and the pulsed oxidizing source, *i.e.* N_2O, during the PRCLA process. Films grown in 8×10^{-4} mbar O_2 background are dark and mirrorlike. The amount of deposited material is mainly controlled by the number of pulses on the target. With, *e.g.* 20 000 pulses films with a thickness of 180–200 nm (Table 1) are obtained. In the case of LCCO on stainless steel the roughness of the deposited film is affected by the deposition temperature. At higher temperatures rough films with many defects are formed. The film thickness on MgO substrates was studied as a function of the substrate–target distance. When this distance is increased by 6 mm from a starting value of 3.7 cm, only 1/3 of the material is deposited with the same number of laser pulses, due primarily to the fact that the substrate is now at a larger angle to the plume axis. For both target/substrate distances films identical stoichiometry are obtained. The roughness of the deposited film increases with increasing film thickness and decreasing target–substrate distance.

Table 1 Thickness and roughness of the LCCO films and different substrates

Condition	Thickness/ nm	Roughness/ nm	Substrate roughness/ nm
LCCO deposited on SS at 560 °C	184	28	13 (SS)
LCCO deposited on SS at room temperature	185	12	
LCCO deposited on MgO at 650 °C at 4.3 cm	65	1.8	4 (MgO)
LCCO deposited on MgO at 650 °C at 3.7 cm	205	2.7	
LCCO deposited on MgO at 650 °C at 3.7 cm	584	4.5	

The stoichiometry of the film was analyzed by RBS (Fig. 3) and the data are summarized in Table 2. A detailed analysis of the La-signal suggests a heterogeneous distribution of this element through the film, *i.e.* a smaller amount of La at the interface than in the bulk. This heterogeneity increases also the error in the determination of the other elements. From most measured LCCO films a typical oxygen content between 2.7 and 3 (±7%) is obtained. This suggests that it is possible to obtain films without oxygen deficiency. It has been suggested by Boyd *et al.*[15] that incongruent transfer occurs during the

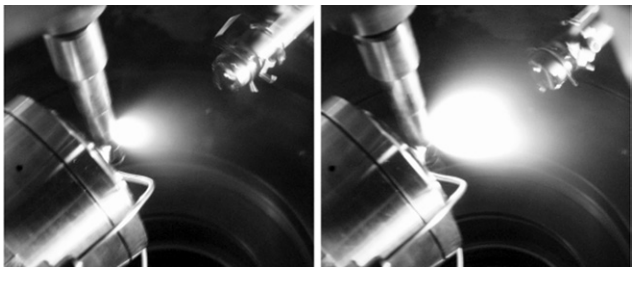

Fig. 2 Photo of the ablation plume without (left) and with (right) N_2O gas pulse.

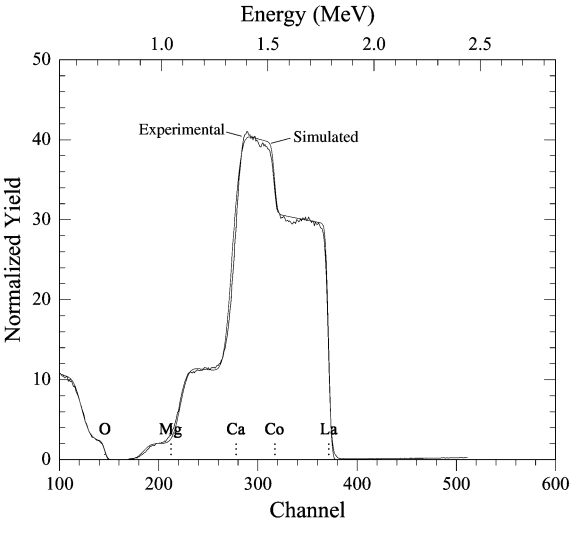

Fig. 3 RBS spectra of a 200 nm LCCO film deposited on MgO(001). Black line: experimental spectrum; red line: simulated spectrum.

Table 2 Stoichiometry of the LCCO films obtained from RBS

Conditions	Stoichiometry
Before 8×10^5 pulses	$La_{0.64 \pm 0.04}Ca_{0.35 \pm 0.02}Co_{0.95 \pm 0.05}O_{3 \pm 0.21}$
After 1.5 Mio. pulses	$La_{0.72 \pm 0.04}Ca_{0.28 \pm 0.02}Co_{0.99 \pm 20.05}O_{2.7 \pm 0.21}$
After mechanical polishing of the target	$La_{0.64 \pm 0.04}Ca_{0.35 \pm 0.02}Co_{0.95 \pm 0.05}O_{3 \pm 0.21}$

PLD process of $La_{1-x}Ca_xMnO_3$ (LCMO) depending on the deposition temperature. In the case of LCCO, we did not observe this incongruent material transfer. Up to around 8×10^5 pulses films with the same stoichiometry as the target were obtained ($La_{0.6}Ca_{0.4}CoO_3$). Then a depletion of Ca (enrichment of La) was detected in the target and the films. The analysis of films and target gave the same composition for both, again confirming the congruent material transfer.

The original target stoichiometry could be regained by mechanical polishing of the target. This suggests that only the surface layer of the target was Ca depleted.

Fig. 5 Pole figure of a LCCO film deposited on MgO(001).

B. Characterization

Analysis of the LCCO films by XRD reveals the formation of the crystalline perovskite phase. A clear influence of the cooling condition on the crystallinity is detected. When the films, grown on MgO at 650 °C with a laser fluence of 7 J cm^{-2} and an oxygen background of 8×10^{-4} mbar, are cooled in the absence of oxygen, only the LCCO(200) peak at 33.18° is observed (Fig. 4A). In the case of cooling in an oxygen background (8×10^{-4} mbar), two peaks are observed (LCCO(200) and LCCO(110), shown in Fig. 4B). The reason for this behaviour is not clear at the moment. The appearance of the LCCO(200) peak in all measurements suggests that the LCCO is preferentially orientated in the (200) direction of the MgO. For LCCO films deposited on SS at 560 °C, (fluence of 7 J cm^{-2}, oxygen background of 8×10^{-4} mbar and cooled in the absence of oxygen) the LCCO(110) at 42.1°, the LCCO(200) at 61.5° and the LCCO(211) at 78.3° peaks are observed. For film grown at room temperature (other experimental conditions the same as before) no crystalline perovskite film was obtained, indicating that only amorphous material was formed.

Fig. 5 shows the (111) pole figure of the LCCO-film at a 2θ angle at 42.97°. In the figure four maxima at $\chi = 54°$ are visible, indicative of the single crystalline domains of the orientated film.

The full width at half maximum (FWHM) of the LCCO(200) rocking curve, that characterizes the quality of the *c*-axis orientation, ranges between 0.13 and 0.9° for the produced films (single crystalline MgO substrates showed a FWHM of 0.1°). In general, better film qualities are obtained when the cooling procedure was performed without oxygen, independent of the cooling rate.

TEM studies were performed to obtain more information about the fine structure of the LCCO films on MgO. A low magnification bright-field TEM image of the cross-section sample (see Fig. 6A) reveals a columnar microstructure of the LCCO film. Scanning electron micrographs (see Fig. 6B) of the surface morphology shows a rough surface. The first layers of the LCCO seem to grow layer by layer coherently (see also HRTEM) regardless of the large lattice misfit (10%) of the LCCO and MgO. In this region the strain is possibly absorbed by the substrate and the film. Above 30–70 nm film thickness the growth mode of the LCCO film seems to change. The areas with different contrast in the HRTEM picture suggest that the film is formed by coalescence of growing epitaxial islands.

Diffraction patterns obtained from the cross-section samples (Fig. 7A) show reflexes produced from the LCCO film and the MgO substrate, confirming the epitaxial growth of the LCCO films in the *c*-direction of the MgO substrate. The index of the LCCO diffraction pattern is based on a cubic symmetry with $a = 3.789$.

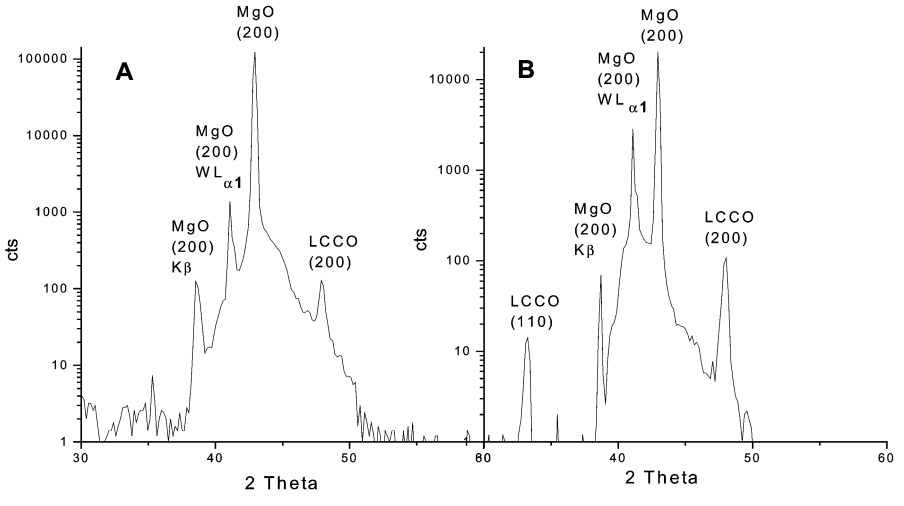

Fig. 4 θ–2θ XRD spectra of LCCO. (A) fast cooling without O_2 background; (B) fast cooling with O_2 background.

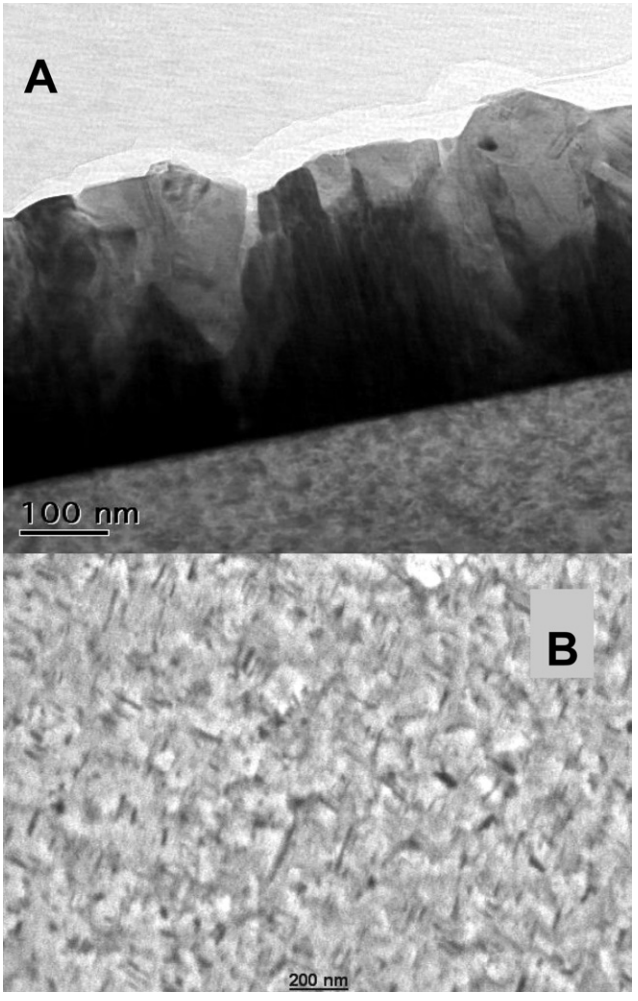

Fig. 6 (A) Low magnification TEM image of the cross-section of a LCCO film deposited on MgO(001). (B) SEM image of the LCCO film.

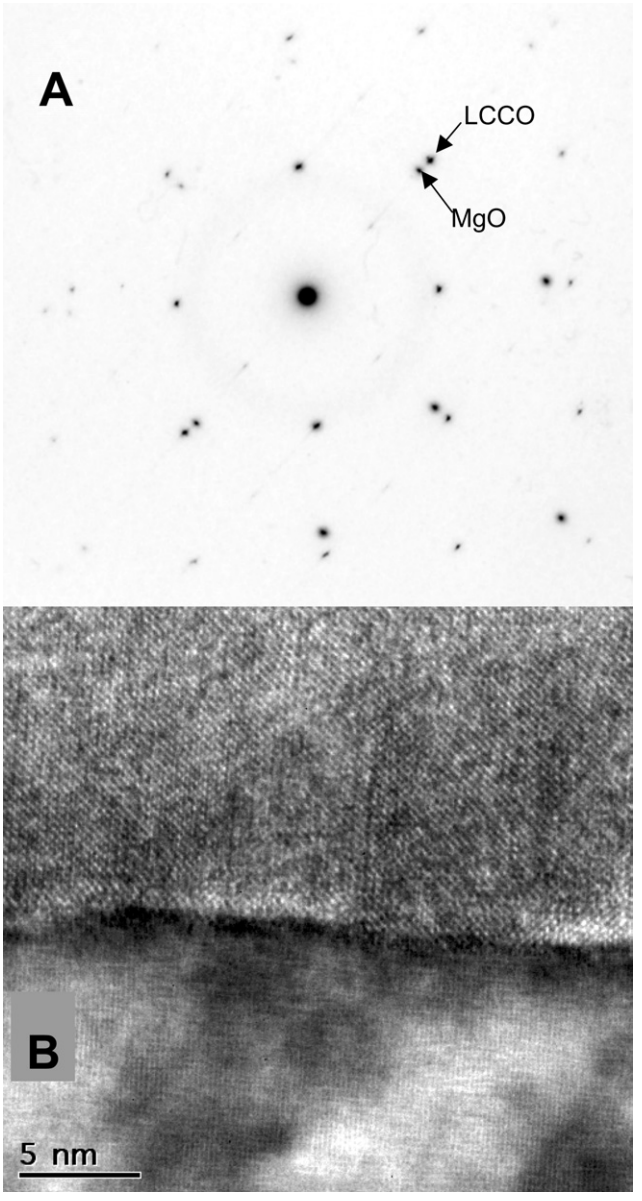

Fig. 7 (A) Electron diffraction of a LCCO film grown on MgO(001). (B) HRTEM image of the LCCO film.

The local structure of the films has been studied by high-resolution electron microscopy to provide structural information on substrate, film and the interface. The HRTEM image shown in Fig. 7B, represents the MgO substrate (lower part) and the LCCO-film (upper part). The layer is quite flat (roughness <1 nm) and no dislocations or secondary phases are visible along the interface.

The lattice spacing measured along the *c*-axis on the image reveals that the contrasts have originated only from the LCCO structure. EDX measurements show that the composition of the LCCO film is $La_{0.6}Ca_{0.4}CoO_3$. Apart from the highly ordered regions in the films, we observed that the top layers are amorphous. These amorphous layers are observed in all samples and result from the ion bombardment during the preparation of the cross-section specimen.

The characterization of the films grown under different conditions (*e.g.* cooling conditions and substrate material/temperature) confirm that the crystallinity of the films can be varied over a broad range, *i.e.* from amorphous over polycrystalline to single crystalline. This control gives the unique opportunity to study the electrocatalytic activity as a function of crystallinity.

C. Surface characterization

Another extremely important parameter for electrocatalysis is the surface composition of the films and the influence that the film preparation may have on the surface composition. Two effects—deposition temperature and substrate material—were analyzed. The survey spectrum of a $La_{0.6}Ca_{0.4}CoO_3$ film on MgO at room temperature is shown in Fig. 8. The

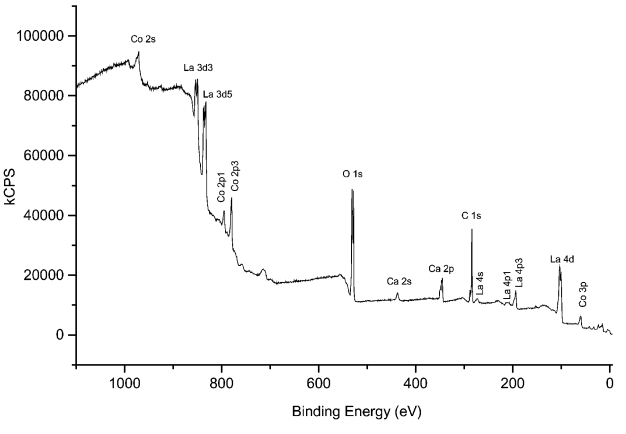

Fig. 8 XPS survey spectra of the LCCO film.

characteristic lines for La, Ca, Co and O are present, showing that except for adventitious carbon the surfaces are free from any contamination. Table 3 summarises the dominant peak

Table 3 Binding energy (eV) of the core levels of $La_{0.6}Ca_{0.4}CoO_3$

Condition	O1s	Ca2p	Co2p3	La 3d5/2
LCCO deposited on SS at room temp.	531.1	346.6	780.1	834.6
LCCO deposited on SS at 560 °C	531.1	345.1	779.6	833.1
LCCO deposited on MgO at 600 °C	531.6	347.1	779.6	833.1
LCCO deposited on SS at 600 °C	531.1	345.1	779.6	833.1
LCCO deposited on Au at 600 °C	529	345.6	780	833.5
LCCO deposited on SS before ER	531.2	344.8	779.3	834.6
LCCO deposited on SS after ER	531	346.7	780	834.5
LCCO deposited on MgO before ER	531.6	347.1	779.6	833.1
LCCO deposited on MgO after ER	531.1	345.6	779.6	834.1

positions for O 1s, Ca 2p, Co $2p_{3/2}$ and La 3d for the different conditions.

C.1 Effect of deposition temperature and substrate. LCCO films were deposited on stainless steel at room temperature and at 560 °C. The XPS spectra of the Ca 2p, O 1s, Co $2p_{3/2}$ and La 3d peaks of a LCCO films, are shown in Fig. 9. Two doublets with peak energies around 345 and 347 eV for the Ca $2p_{3/2}$ signal were obtained. This suggests that two calcium species are present on the film surface. In the O 1s spectrum again two peaks are observed at *ca.* 528 and *ca.* 531 eV, indicating the presence of two oxygen species. To clarify the origin of these two species angle resolved studies were performed. A comparison of, *e.g.*, two Ca 2p spectra, one measured at normal emission and the other at 45°, shows an increase of the peak at higher binding energy. Therefore, the peak at higher binding energy is related to a top layer and the one at lower binding energy to the bulk film. This is the case for the Ca 2p, O 1s and La 3d peaks, but it is not visible for the Co $2p_{3/2}$ peak. The spectra also reveal that the peaks of Ca and O are related and have most probably the same origin. The surface species could correspond to CaO [16] and/or oxygen physisorbed on the surface[17] and/or $CaCO_3$. The latter is supported by a small peak around 289 eV in the C1s spectra, which can be assigned to a carbonate.[16] In the Co $2p_{3/2}$ spectra only one peak around 780 eV is observed, which is assigned to Co^{3+}.[18] The La $3d_{3/2}$ and La $3d_{5/2}$ are split into two components of comparable intensities due to the presence of inequivalent La atoms.[18]

The temperature effect can be clearly observed in the Ca 2p and O 1s spectra. A maximum peak intensity of the surface species is observed when the films are grown at room temperature (RT). For a deposition temperature of 560 °C the intensity of the surface peaks decreases and the peaks, due to the perovskite structure, increase to become the peaks with the highest intensity. This suggests that the substrate temperature used during the deposition directly influences the thickness of the surface species layer on the film. In the case of Co the same peak is observed for both deposition temperatures but a difference in peaks width is evident. The FWHM of a peak can be influenced by two factors, *i.e.* conductivity and crystallinity. It is known that better crystallinity leads to peaks with smaller FWHM values. In other words, the peak for the films grown at 560 °C (polycrystalline film) should present the smaller FWHM compared to the amorphous film grown at RT. In

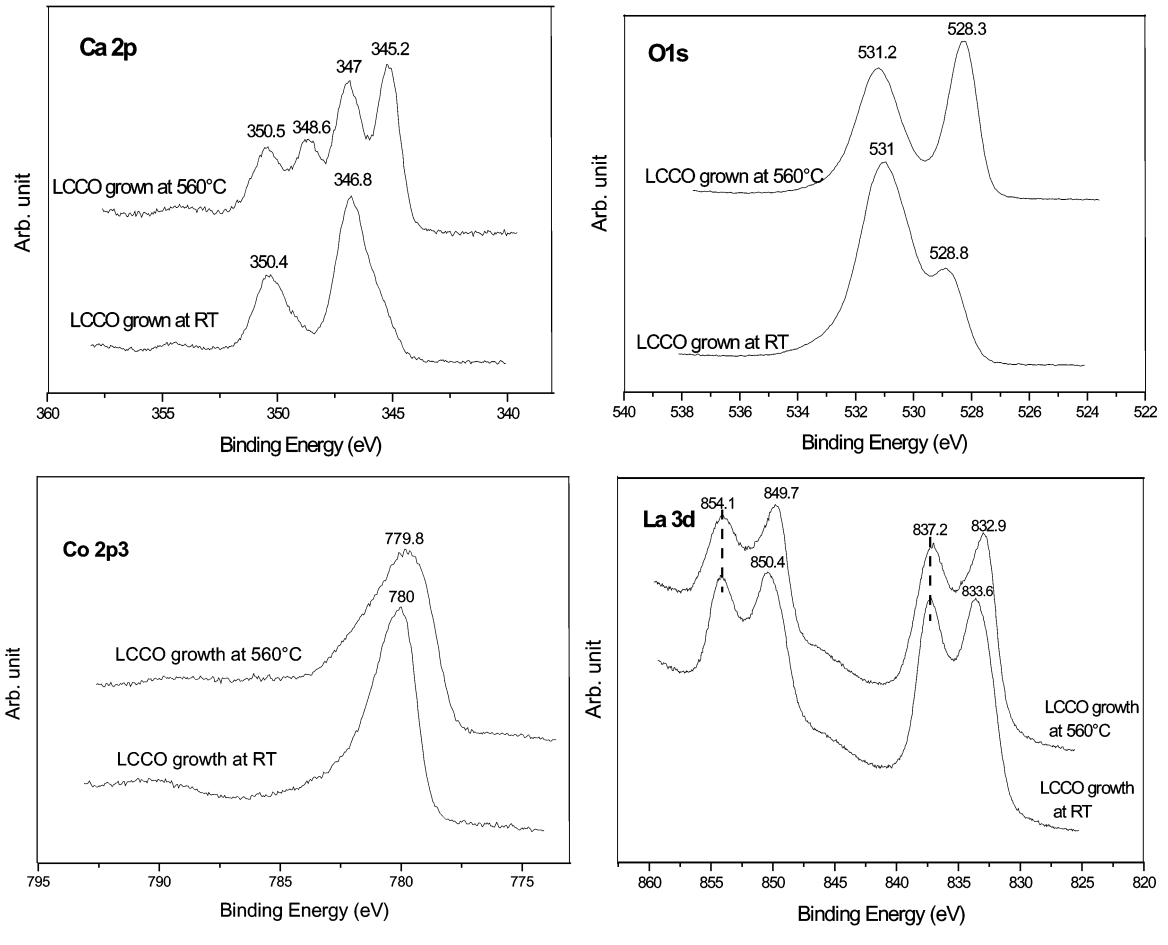

Fig. 9 XPS spectra of Ca 2p, O 1s, Co $2p_{3/2}$ and La 3d peaks of LCCO film grown on stainless steel at RT and 560 °C.

our experiments the opposite behavior is observed. The conductivity (not measured so far) should remain the same, because the films have the same stoichiometry and are grown on the same substrate. Another possibility could be a broadening of the peaks due to the existence of two species. The La $3d_{3/2}$ and $3d_{5/2}$ peaks are present for both deposition temperatures, but reveal an asymmetry due to two species. The fact that two La species are observed, suggests also that in the case of Co two species are present. The origin and composition of these species are not known at the moment.

Three substrates were used for the film deposition, *i.e.* stainless steel, gold and MgO(001). The films were grown at 560 °C, 650 °C and 650 °C, respectively. The general features of the peaks are the same as described above. For Ca and O a difference in the maximum peak intensity is observed. On MgO the maximum peak intensities are due to the surface species. For films deposited on SS and Au the surface peaks decrease and the peak due to the perovskite structure increases to reach the maximum intensity. This suggests, that the substrate properties have also an influence on the surface composition, probably due to the different crystalline structure which is obtained for the different substrates. Another possible explanation could be the different conductivity of the substrates.

D. Electrochemical measurements

To study the electrochemical activity of the LCCO material (powder and films) polarization curves under steady state conditions were measured (shown in Fig. 10A and B, respectively). A gas diffusion electrode has been prepared to measure the activity of the LCCO powder. For this type of electrode the catalyst powder was mixed with carbon and PTFE. In alkaline electrolyte the carbon as well as the catalyst show a certain activity for oxygen reduction and evolution. Fig. 10 shows voltage *vs* current density plots for the carbon and different LCCO–carbon mixtures. The curves reveal that the carbon (Vulcan XC 72) without catalyst presents activity for both oxygen reactions. The potential at which the oxygen evolution reaction takes place drops by a value of *ca.* 0.5 V when the catalyst is added to the carbon, indicating an activity enhancement of the electrode for this reaction. Special treatment of the carbon in order to improve its active surface area and wettability leads to further improvement of the current potential behavior of the electrode. Additional improvement of the electrode could be demonstrated by optimizing the thickness of the active-layer (containing the catalyst) and thus diminishing the diffusion length for oxygen diffusion to the reactive sites. These examples show the sensitivity of the electrode performance to engineering parameters and the resulting problem to estimate the influence of the catalyst on the overall electrochemical activity of these electrodes. This shows why it is necessary to prepare thin films when the aim of the study is the reaction mechanism. Only for dense films will the observed catalytic activity correspond to the catalyst and the active area of the electrode can be easily determined. One parameter which can only be studied with PLD films is the influence of the crystallinity on the catalytic activity. Therefore, one film deposited on MgO (single crystalline film) and another deposited on stainless steel (polycrystalline film) were selected (Fig. 10B) to study the electrochemical properties, as function of the crystallinity. The single crystalline film on MgO reveals a lower potential for the oxygen evolution than the polycrystalline LCCO film electrode and a higher current density for oxygen reduction conditions. These results confirm that the crystallinity has an influence on the activity of LCCO. In our case, a better performance for single crystalline films is observed. The single crystalline films are even better than the most advanced gas diffusion electrodes (see Fig. 10B) confirming the importance of the LCCO catalyst.

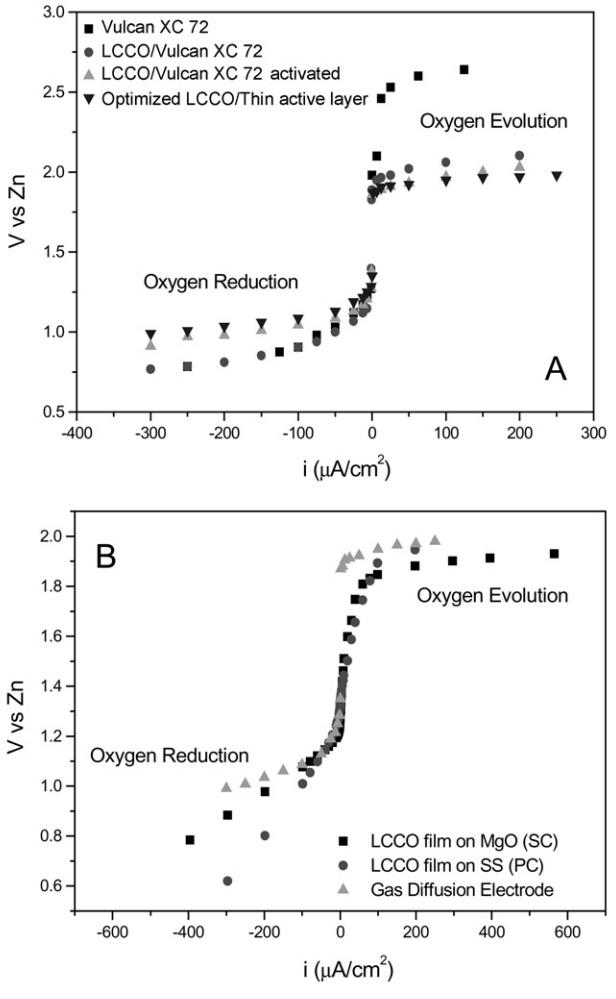

Fig. 10 Current density *vs* potential curves: (A) for various gas diffusion electrodes; (B) for LCCO PLD film and gas diffusion electrodes.

Conclusion

Perovskite films ($La_{0.6}Ca_{0.4}CoO_3$, LCCO) were grown on various substrates by pulsed reactive crossed beam laser ablation. The characterization of the films reveals that it is possible to control the crystallinity of the films by varying the deposition temperature, substrate material and cooling conditions. It was possible to obtain films ranging from single crystalline to amorphous. This control is important for a correlation of crystallinity with catalytic activity and for fundamental studies of the catalyst that can be implemented in the engineering design of air based batteries. The surface analysis of the film suggests that surface species containing Ca and O are present. The amount of these surface species depends on the deposition temperature and substrate material. Single crystalline films revealed a higher catalytic activity for oxygen reactions than polycrystalline films.

Acknowledgement

The authors would like to thank Roland Wessiken, ETH Zürich, for his help in the transmission microscopic studies.

References

1 J. T. Cheung, P. E. D. Morgan, D. H. Lowndes, X. Y. Zheng and J. Breen, *Appl. Phys. Lett.*, 1993, **62**, 2045.
2 S. Müller, F. Holzer and O. Haas, *J. Appl. Electrochem.*, 1998, **28**, 895.

3 L. G. Tejuca, J. L. Fierro and J. M. D. Tascón, *Adv. Catal.*, 1989, **36**, 237.
4 S. K. Tiwari, S. P. Singh and R. N. Singh, *J. Electrochem. Soc.*, 1996, **143**, 1505.
5 J. B. Goodenough and R. Manoharan, *Electrochemical Society Proceedings*, 1992, **92**, 11.
6 Y. Shimizu, K. Uemura, H. Matsuda, N. Miura and N. Yamazoe, *J. Electrochem. Soc.*, 1990, **137**, 3430.
7 S. Müller, O. Haas, C. Schlatter and C. Comninellis, *J. Appl. Electrochem.*, 1998, **28**, 305.
8 P. R. Willmott and J. R. Huber, *Rev. Mod. Phys.*, 2000, **72**, 1.
9 D. Bäuerle, *Laser Processing and Chemistry*, Springer Verlag, Berlin, 3rd edn., 2000.
10 P. R. Willmott, R. Timm and J. R. Huber, *J. Appl. Phys.*, 1997, **82**, 2082.
11 L. C. Feldman and J. W. Mayer, *Fundamentals of Surface and Thin Film Analysis*, North Holland, 1986.
12 L. R. Doolittle, *Nucl. Instrum. Methods*, 1986, **B15**, 227.
13 H. Arai, S. Müller and O. Haas, *J. Electrochem. Soc.*, 2000, **147**, 3584.
14 D. B. Chrisey and G. K. Hubler, *Pulsed Laser Deposition of Thin Films*, John Wiley & Sons, New York, 1994.
15 I. W. Boyd and W. Zhang, *Appl. Surf. Sci.*, 1998, **410**, 127.
16 C. D. Wagner, W. M. Riggs, L. E. Davis and J. F. Moulder, *Handbook of X-ray photoelectron spectroscopy*, ed. G. E. Muilenberg, Perkin Elmer Corporation, 1979.
17 V. Craciun and R. K. Singh, *Appl. Surf. Sci.*, 2000, **168**, 239.
18 P. Wang, L. Yao, M. Wang and W. Wu, *J. Alloys Compd.*, 2000, **311**, 53–56.